

See discussions, stats, and author profiles for this publication at: <https://www.researchgate.net/publication/259199712>

Oxygen Isotope Composition of Trinitite Postdetonation Materials

ARTICLE *in* ANALYTICAL CHEMISTRY · DECEMBER 2013

Impact Factor: 5.64 · DOI: 10.1021/ac402757p · Source: PubMed

CITATIONS

3

READS

36

4 AUTHORS, INCLUDING:



[Antonio Simonetti](#)

University of Notre Dame

182 PUBLICATIONS 3,123 CITATIONS

[SEE PROFILE](#)



[Wei Chen](#)

China University of Geosciences

10 PUBLICATIONS 59 CITATIONS

[SEE PROFILE](#)



[Peter C Burns](#)

University of Notre Dame

490 PUBLICATIONS 8,363 CITATIONS

[SEE PROFILE](#)

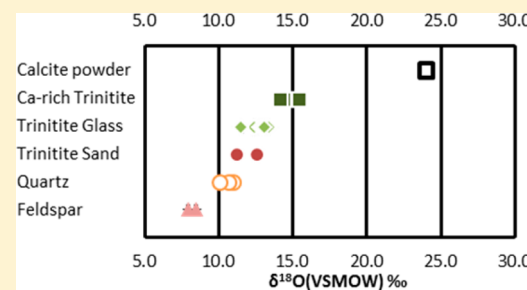
Oxygen Isotope Composition of Trinitite Postdetonation Materials

Elizabeth C. Koeman,* Antonio Simonetti, Wei Chen, and Peter C. Burns

Department of Civil Engineering and Environment Engineering and Earth Sciences, University of Notre Dame, Notre Dame, Indiana 46556, United States

Supporting Information

ABSTRACT: Trinitite is the melt glass produced subsequent the first nuclear bomb test conducted on July 16, 1945, at White Sands Range (Alamagordo, NM). The geological background of the latter consists of arkosic sand that was fused with radioactive debris and anthropogenic materials at ground zero subsequent detonation of the device. Postdetonation materials from historic nuclear weapon test sites provide ideal samples for development of novel forensic methods for attribution and studying the chemical/isotopic effects of the explosion on the natural geological environment. In particular, the latter effects can be evaluated relative to their spatial distribution from ground zero. We report here $\delta^{18}\text{O}(\text{\textperthousand})$ values for nonmelted, precursor minerals phases (quartz, feldspar, calcite), “feldspathic-rich” glass, “average” melt glass, and bulk (natural) unmelted sand from the Trinity site. Prior to oxygen isotope analysis, grains/crystals were examined using scanning electron microscopy (SEM) and energy dispersive X-ray spectroscopy (EDS) to determine their corresponding major element composition. $\delta^{18}\text{O}$ values for bulk trinitite samples exhibit a large range (11.2–15.5‰) and do not correlate with activity levels for activation product ^{152}Eu ; the latter levels are a function of their spatial distribution relative to ground zero. Therefore, the slow neutron flux associated with the nuclear explosion did not perturb the $^{18}\text{O}/^{16}\text{O}$ isotope systematics. The oxygen isotope values do correlate with the abundances of major elements derived from precursor minerals present within the arkosic sand. Hence, the O isotope ratios documented here for trinitite melt glass can be attributed to a mixture of the respective signatures for precursor minerals at the Trinity site prior to the nuclear explosion.



Stable isotope analysis is a valuable geochemical technique for delineating the circumstances of formation and origin for most rock types.¹ Significant differences in oxygen isotope values exist between sedimentary and igneous rocks as a result of interactions and redistributions that have occurred since their formation.² Oxygen isotopic signatures can also be characteristic of postsolidification, temperature-induced alteration and can help constrain the parameters of such an event.³ Numerous, previous studies exist in the literature that utilize well established temperature-dependent fractionation factors between a pair of cogenetic minerals to determine the temperature of the last equilibration within a rock system.^{4–6} Variations in the $\delta^{18}\text{O}$ values between minerals formed within igneous systems are typically small such that analytical techniques yielding high precision are needed to distinguish the differences.¹ The laser fluorination method is one such technique and was employed in this study to delineate $\delta^{18}\text{O}$ values within postdetonation materials resulting from the world’s first nuclear bomb explosion, Trinity.

The Trinity nuclear weapon, which consisted of a plutonium implosion device, was hoisted to a height of 30 m on a steel tower at ground zero (GZ) within the White Sands Missile Range (New Mexico, USA). Upon detonation at 5:29:45 a.m. on July 16, 1945, the temperature at GZ was estimated to be >1470 °C⁷ and the fireball temperature to be ~8160 °C.⁸ Subsequent device detonation, components of the steel tower and bomb along with natural materials from the desert were

swept up into the fireball. Radionuclides, including unfissioned Pu, fission products, and neutron activation products were also entrained into the cloud.⁹ The entire process resulted in the formation of a glassy, green colored material referred to as “Trinitite”. A two-step formation mechanism has been proposed for trinitite,^{10,11} which involved generation of molten glass both on the ground and in the mushroom cloud during the first stage; this was followed by the incorporation of solid material (nonmolten mineral phases, metal, and droplets) raining down from the cloud on the upper surface of the solidifying glass. Of note, the prevailing arid conditions of New Mexico’s desert have likely prevented mobilization and leaching of many long-lived radionuclides in the ~68 years since the explosion.¹² However, secondary clay minerals have formed (as discussed below) subsequent the time of the nuclear detonation.

The natural materials from the geological background within trinitite prove to be an important component during forensic analysis.^{9,13} Minerals present within the local arkosic sand include quartz, feldspars (microcline and albite plagioclase), carbonates, sulfates, chlorides, hornblende, olivine, and clay minerals kaolinite and Illite.^{7,8,14} These unmelted components are located predominantly within the nonglassy (bottom) side

Received: August 22, 2013

Accepted: November 27, 2013

Published: December 5, 2013

of most trinitite samples and in general were not affected by the explosion (Figure 1). There are two distinct types of glass that



Figure 1. Samples of trinitite with the top image (A) illustrating the melted surface, whereas (B) displays a sandy bottom characterized by loosely bound materials.

make up trinitite: a silica-rich glass resulting from the melting of quartz and a second type emanating from the melting of feldspar and clay minerals⁷ (Figure 2).

It is important to note that, during nuclear explosions, fission products are formed by the thermal neutron-induced fission of ²³⁹Pu (the fuel used in the Trinity device) and other fissile nuclei. In relation to the Trinity test, Wahl modeled the abundances of the fission products, which resulted in a bimodal, asymmetric mass distribution, with the relative proportions of fission products depending on the mass number of the isotope undergoing fission and the speed of the impacting neutrons.¹⁵ Hence, the presence of a neutron flux subsequent to a nuclear explosion may impact the isotope composition of “stable” elements, such as oxygen. The degree of possible perturbation of the inherent stable oxygen isotope ratios for precursor minerals within the desert sand at GZ will be a function of the absorption cross section to thermal neutrons for the pertinent isotopes involved. In this case, ¹⁸O is characterized by an absorption cross section for thermal neutrons of ~0.16 mbarns compared to a similar value of 0.19 mbarns for ¹⁶O (<http://www.ncnr.nist.gov/resources/n-lengths/list.html>). Therefore, the similar absorption cross sections for thermal neutrons for both ¹⁸O and ¹⁶O reduce the likelihood of recording isotope variations that are solely a function of fission and the presence of a slow neutron flux. The validity of this statement is tested in this investigation.

This study focuses on a stable oxygen isotope characterization of trinitite postdetonation materials (PDMs), and to our knowledge, this is the first study to report oxygen isotope ratios for trinitite PDMs. Prior to oxygen isotope analysis via laser fluorination, trinitite materials were investigated in detail for

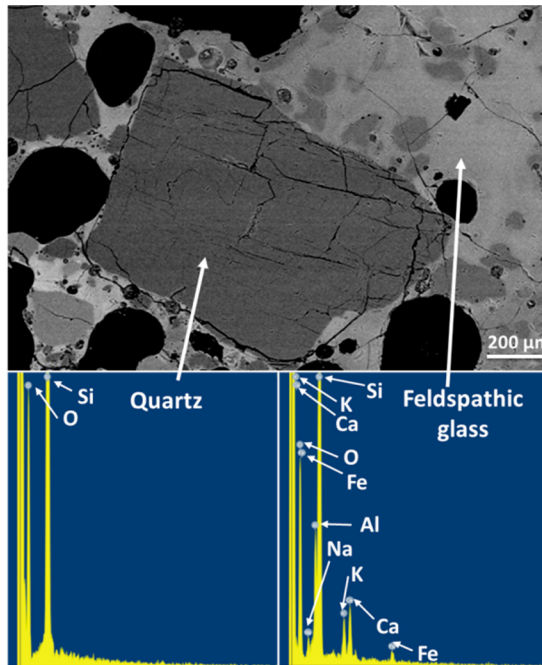


Figure 2. Backscattered electron (BSE) image of trinitite obtained by scanning electron microscopy (SEM). Also shown are the energy dispersive X-ray spectroscopy (EDS) results corresponding to quartz (bottom left photo) and feldspathic melt glasses (bottom right image).

their major element composition via scanning electron microscopy (SEM)—energy dispersive X-ray spectroscopy (EDS) analysis (Figure 3). Moreover, unaltered feldspar grains

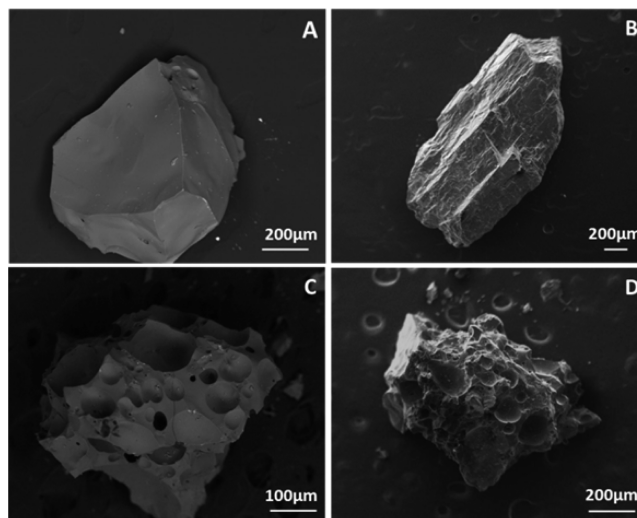


Figure 3. SEM-BSE images of selected trinitite material analyzed for oxygen isotope measurement by laser fluorination. Corresponding chemical compositions can be found in Supporting Information: (A) Sample 4C 6.75-2, (B) Sample 4E 3.18, (C) Sample 5B 10.48, and (D) Sample 5E 2.10.

(taken from the sandy bottom of the samples), as well as the two distinct types of melt glasses (verified by EDS; e.g., Figure 2), were analyzed for their oxygen isotope compositions. The $\delta^{18}\text{O}$ value for loosely bound carbonate material from the “sandy” (unmelted) side of trinitite samples (e.g., Figure 1) was also investigated. The oxygen isotope results are subsequently evaluated in conjunction with their corresponding major

Table 1. Stable Oxygen Isotope Values for Trinitite Material and Certified Reference Standard Materials

sample	$\delta^{18}\text{O}$ (‰)	±	standard	certified $\delta^{18}\text{O}$ (‰)	$\delta^{18}\text{O}$ (‰)	±
1 5.05	13.45	0.05	Lausanne Quartz-1		18.08	0.07
4A 5.37	15.12	0.08	Lausanne Quartz-2		18.33	0.06
4B 4.92	11.60	0.05	Lausanne Quartz-3	18.15	18.06	0.07
4C 5.33	12.79	0.05	Lausanne Quartz-4		17.95	0.08
4C 6.75-1	13.43	0.07				
4C 6.75-2	10.98	0.09	San Carlos Olivine-1		5.22	0.04
4D 10.44	10.70	0.09	San Carlos Olivine-2	4.9–5.7 ²³	5.25	0.09
4D 2.45	15.36	0.06	San Carlos Olivine-3		5.07	0.09
4D 2.45	10.07	0.05	San Carlos Olivine-4		5.75	0.04
4E 1.04	12.58	0.06				
4E 3.18	13.10	0.07	Reference Oxygen Gas-1	25.79	25.73	0.11
4F 6.30-1	11.54	0.08	Reference Oxygen Gas-2		25.59	0.06
4F 6.30-2	14.35	0.05				
4F 9.36	13.04	0.04	NBS18-1	7.20	7.28	0.07
SB 10.48	12.91	0.03	NBS18-2		7.17	0.04
SC 7.68	12.82	0.06				
SD 1.57	13.41	0.06	NBS19-1	28.65	28.75	0.03
SD 1.78	13.07	0.07	NBS19-2		28.79	0.08
SD 1.94	12.93	0.06				
SE 1.47	13.05	0.02	LSVEC-1	3.69	3.77	0.06
SE 2.10	13.14	0.06	LSVEC-2		3.79	0.07
SE 2.44-1	15.73	0.08				
SE 2.44-2	13.51	0.06				
Calcite (powder)	24.81	0.03				
Quartz Glass	10.59	0.07				
K-Feldspar	8.2	0.15				

element compositions and their spatial distribution relative to ground zero; the latter is based on the bulk sample ^{152}Eu activity determined by gamma spectroscopy.¹⁶ This comparison will provide some insights as to the applicability of $\delta^{18}\text{O}$ values as a potential forensics tool in future studies of PDMs, in particular for providing insights into deciphering possibly complex chemical signatures.

SAMPLES AND ANALYTICAL METHODS

Samples. Trinitite samples investigated here were purchased from the Mineralogical Research Corporation (<http://www.minresco.com>) and belong to different morphological groups based on inclusion types (Figure 1, see Supporting Information).

Scanning Electron Microscopy (SEM). Fragments of trinitite were ground using an agate mortar and pestle in order to produce millimetric-sized materials/grains. Approximately 2–5 grains were carefully hand-picked using a petrographic microscope so as to select material of a similar (petrographic/mineralogical) nature for each sample; this typically yielded a total sample weight of between 1.0 and 1.9 mg. Individual grains were examined in detail with a Leo scanning electron microscope (SEM) using energy dispersive X-ray spectroscopy (EDS; Figure 3) in order to determine major element abundances (provided in Supporting Information). EDS analyses were conducted using an accelerating voltage of 20 kV and spot size of 500 μm .

Stable Oxygen Isotope Analysis. Stable O isotopic ratios of trinitite were obtained using a MIR-10 CO₂-based laser (ESI-New Wave) fluorination system coupled to a silicate extraction line (after Sharp¹) and slightly modified for operation in continuous flow mode. With the aid of a binocular microscope, samples are loaded into separate tapered holes ($n = 44$ in total)

within a nickel block. The block is housed within a stainless steel chamber with a BaF₂ glass window that is inert to fluorine gas. Upon entering the stainless steel chamber, BrF₅ is reacted with the samples using a 20W CO₂ laser operating in continuous wavelength mode and a beam size of 1.6 mm for heating purposes. This reaction liberates the O₂ gas along with other gaseous components. The oxygen gas is purified along a stainless steel extraction line containing various “traps/filters”, i.e., both liquid nitrogen cooled and heated, halite-bearing (neutralizing) types. The O₂ gas is subsequently collected into a frozen, septum-covered quartz vial that is lined at the bottom with millimetric-sized zeolite-coated ceramic vacuum beads; these are kept overnight in an oven at >100 °C prior to placement in the quartz vial so as to minimize blank and moisture levels. The frozen quartz vial (and ceramic beads contained therein) is subsequently heated, and the O₂ gas is then mixed with high purity He gas (for pressurization). The septum is then pierced with a sample probe, and the O₂ and He mixture enters a gas chromatographic (GC) capillary column (kept at 50 °C) housed within a Gas Bench II inlet system and is coupled to the isotope ratio mass spectrometer. Oxygen isotope values were measured using a Delta V Advantage mass spectrometer (Thermo Fisher Scientific) located within the Center for Environmental Science and Technology (CEST) facility at the University of Notre Dame. The daily instrument calibration routine involves analyzing an oxygen reference gas that is calibrated against the NBS 19 standard (certified $^{18}\text{O}/^{16}\text{O} = 28.79\text{\%}$) at both the beginning and the end of each analytical session. An individual isotope ratio measurement consists of analyzing 2–10 s injections each of the reference gas (separated by 40 s interval), which is then followed by 10 injections (each 10 s, also separated by a 40 s interval) of gas from either sample or standard generated by the laser

fluorination process. An average isotope ratio measurement is calculated and reported in $\delta^{18}\text{O}$ (\textperthousand) notation relative to standard mean ocean water (SMOW).¹⁷ Instrumental mass fractionation and instrument drift was monitored by repeated and systematic analysis of the synthetic Lausanne Quartz (certified $^{18}\text{O}/^{16}\text{O} = 18.15\text{\textperthousand}$)¹⁸ using a “sample-standard” bracketing technique during each analytical session. Two standards were analyzed at the start of each session, followed by 5 unknowns, one standard, 5 unknowns, and ending with 2 standards. Each sample takes approximately 2 min to fluorinate, followed by ~20 min for O_2 gas purification and extraction and then isotope ratio measurement. Each standard and unknown sample was measured once. In addition, ~1 mg mineral fractions of pure San Carlos olivine were periodically analyzed during the course of each analytical session as a secondary standard in order to validate the isotope results. The $\delta^{18}\text{O}$ values for the analyses of the San Carlos olivine overlap the range recently obtained by SIMS (secondary ion mass spectrometry) by Eiler et al.¹⁹ Moreover, several aliquots of an oxygen reference gas ($^{18}\text{O}/^{16}\text{O} = 25.79\text{\textperthousand}$) provided by Professor Z. Sharp (University of New Mexico) were periodically injected into the quartz vial with a sterile syringe, and their analyses yielded values either identical or just slightly below the certified value. Subsequent both sample and standard analyses, the zeolite-coated ceramic beads are heated with a heat gun (5–10 min) in order to drive off any residual gas so as to avoid memory effects or cross contamination. The residual gas is evacuated using a primary rotary pump system containing a large cold trap. The residual gas removal process and vacuum integrity of the O_2 capture system is monitored via an online vacuum gauge located proximal to the quartz vial. The ceramic beads are replaced periodically so as to ensure an effective level of capture of the oxygen gas and maintain low blank levels.

The $^{18}\text{O}/^{16}\text{O}$ measurement for loosely bound carbonate found on the “sandy” (bottom) side of trinitite was determined using the standard orthophosphoric acid digestion method and the IR-MS Delta V Advantage mass spectrometer. Replicate analyses of NBS 19 standard (certified $^{18}\text{O}/^{16}\text{O} = 28.65\text{\textperthousand}$) and NBS-18 (certified $^{18}\text{O}/^{16}\text{O} = 7.20\text{\textperthousand}$) are listed in Table 1. The measured $^{18}\text{O}/^{16}\text{O}$ ratio for the calcite was calculated according to the two-point linear normalization by Paul et al.²⁰

X-ray Diffraction. Prior to analysis, the white powder retrieved from the bottom of trinitite samples (e.g., Figure 1) was analyzed on a Bruker D8 Davinci Powder X-ray Diffractometer to determine its phase composition (5–80° 2-theta, step = 0.2, time = 0.5). The diffractometer results confirm that the white powder is composed predominantly of calcite and minor amounts of quartz.

RESULTS

$\delta^{18}\text{O}$ Values of Natural Components. Several previous investigations have shown that the major element composition of trinitite blast melt is highly dependent on the constituent minerals within the precursor arkosic sand present at GZ.^{7,13,14} The major element abundances determined by EDS analysis for the trinitite materials investigated here are listed in the Supporting Information. Overall, the major element abundances overlap those reported in previous trinitite studies.^{8,13,14} Figures 4 and 5 demonstrate the relationships between various major elements within trinitite; in general, both FeO and Na₂O (wt %) abundances correlate with Al₂O₃ contents (Figure 4). Figure 5A compares the wt % contents of SiO₂ and Al₂O₃ for trinitite investigated here, and these define a “mixing” trend

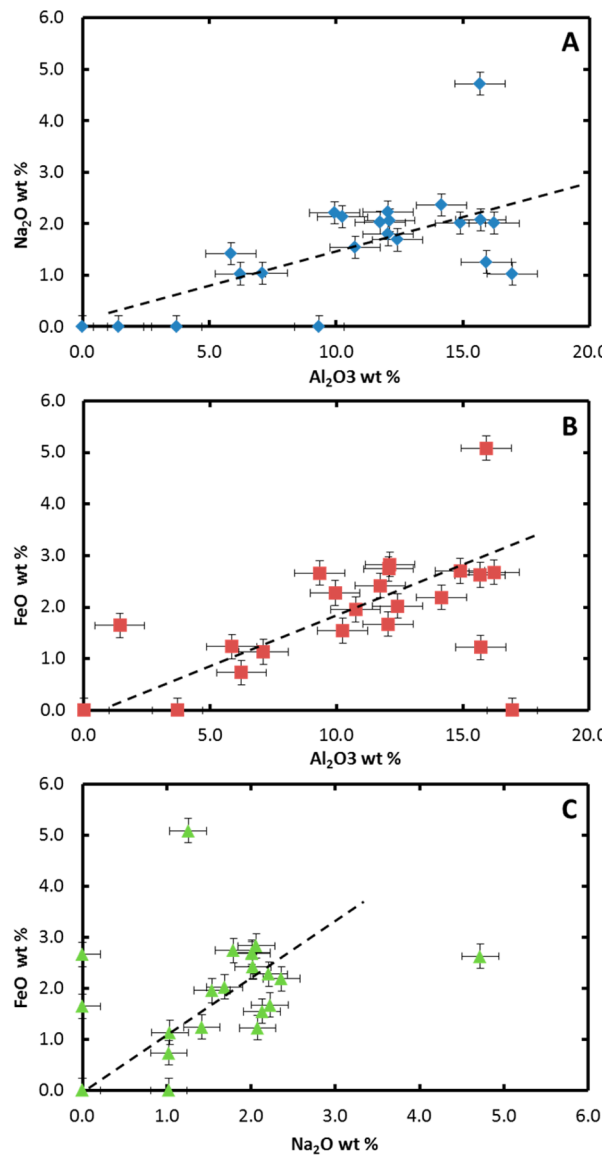


Figure 4. FeO and Na₂O vs Al₂O₃ (A, B) and FeO vs Na₂O (C) contents for trinitite grains investigated here. Error bars are reported at 1 σ level.

between the ideal compositional fields for quartz and plagioclase (and K-feldspar). The Al₂O₃ and CaO wt % abundances of trinitite plot within the triangular area delineated by the compositional fields of quartz, plagioclase, and K-feldspar (Figure 5B).

All of the trinitite materials analyzed here define a significant variation in $\delta^{18}\text{O}$ values, which range between ~8 and ~25‰ (Table 1). In Figures 6 and 7, the abundances of major elements are compared to their corresponding measured $\delta^{18}\text{O}$ (‰) values and several trends are apparent. Figure 6A,B shows the relationship between CaO and SiO₂ wt % abundances against their oxygen isotope values, respectively. Overall, CaO abundances are positively correlated with oxygen values, although there is some scatter (Figure 6A), whereas the latter exhibit a negative correlation with SiO₂ contents (Figure 6B). Also, the oxygen isotope value of calcite (crystal structure verified by XRD analysis), which was easily scraped off the “sandy” (bottom) side of the trinitite samples, is characterized by a high $\delta^{18}\text{O}$ value (24.81‰; Figure 6A). As with results

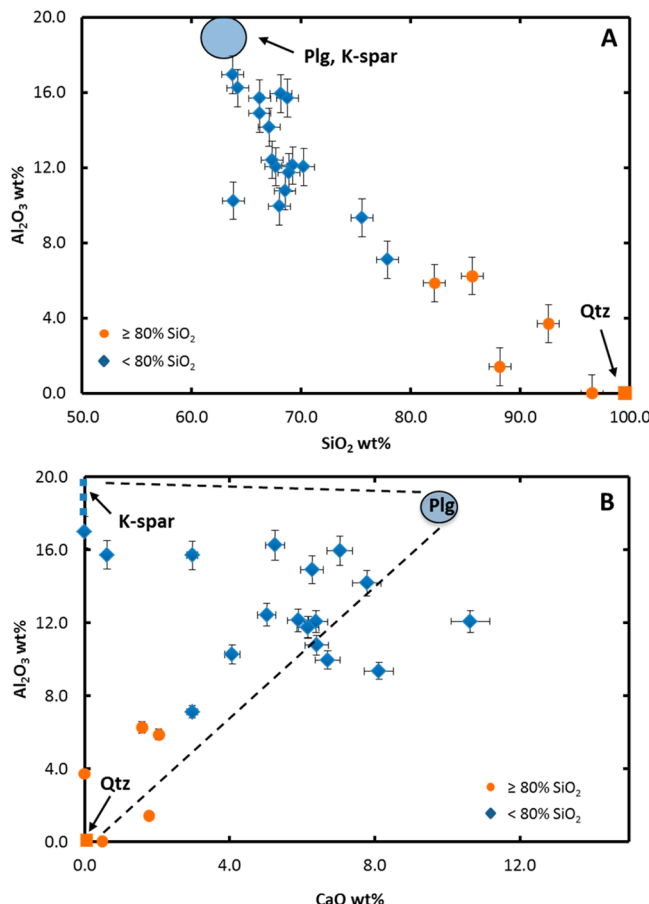


Figure 5. (A) SiO_2 vs Al_2O_3 contents and (B) CaO vs Al_2O_3 abundances for trinitite grains; quartz (Qtz), plagioclase (Plg), and potassium feldspar (K-spar) compositional fields are shown in both plots. Error bars are 1σ .

shown in Figure 6, $\delta^{18}\text{O}$ values are again controlled by end-member mineral compositions (quartz, plagioclase, K-feldspar, calcite) when plotted against both Na_2O and Al_2O_3 wt % abundances (Figure 7).

^{152}Eu Activity vs $\delta^{18}\text{O}$. Prior to oxygen isotope analysis, whole rock trinitite samples employed here were investigated via bulk sample gamma spectroscopy. Details regarding the gamma spectroscopy methods and results are in Bellucci et al.¹⁶ The natural sand at GZ was a source of both naturally occurring isotopes of europium, ^{151}Eu and ^{153}Eu . During the Trinity explosion, the sand was exposed to a large neutron flux as a result of ^{239}Pu ($\pm \text{U}$) fissioning.^{12,16} During the flux, both natural Eu (151 and 153) isotopes underwent a (n,γ) interaction with thermal neutrons to produce ^{152}Eu and ^{154}Eu . Therefore, the abundances of both isotopes can be directly correlated to device-related activity. Figure 8 shows a comparison between bulk sample ^{152}Eu activity and corresponding $\delta^{18}\text{O}$ values for trinitite glass, precursor arkosic sand, and Ca-rich ($\text{CaO} \geq 8$ wt %) trinitite. Trinitite samples have $\delta^{18}\text{O}$ values between 11.2 and 13.5‰ (trinitite glass and sand), whereas Ca-rich trinitite is characterized by heavier $\delta^{18}\text{O}$ values that vary between 14.2 and 15.5‰ (Figure 8).

■ DISCUSSION

The average $\delta^{18}\text{O}$ value for feldspar + clay trinitite melt is $12.94 \pm 0.06\text{\textperthousand}$ ($n = 23$), which is higher compared to both quartz

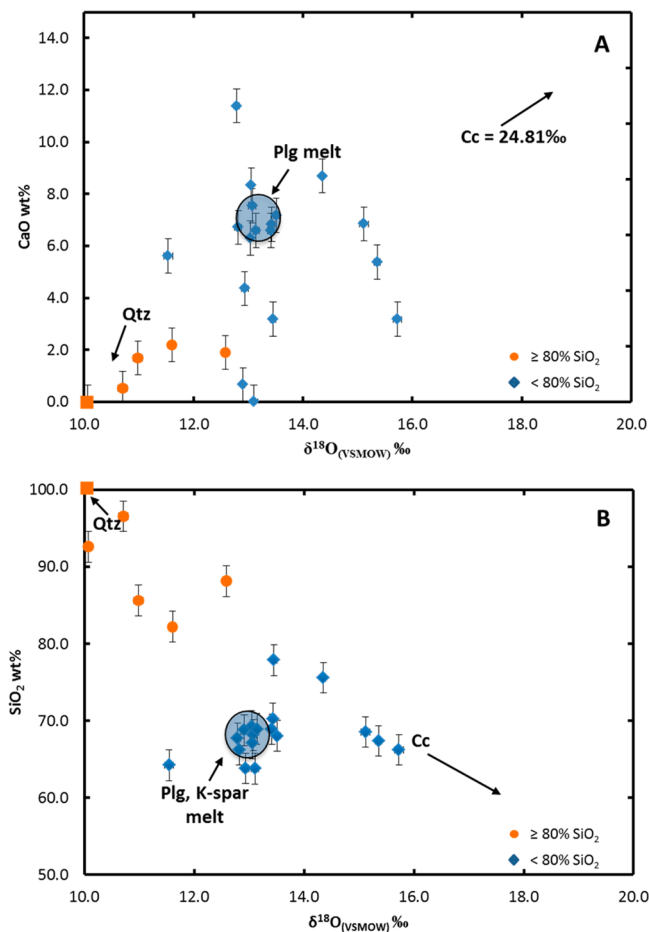


Figure 6. CaO (A) and SiO₂ (B) weight percent vs $\delta^{18}\text{O}$ (in ‰, VSMOW) values of trinitite grains. Compositional fields for quartz (Qtz), feldspar (Plg, K-spar) melt, and calcite (Cc) are shown. Error bars are 1σ .

glass ($10.59 \pm 0.07\text{\textperthousand}$; $n = 3$) and unaltered K-feldspar ($8.2 \pm 0.15\text{\textperthousand}$; $n = 2$). The oxygen isotope values for quartz glass fall within the range of 10–13‰, which is typical for quartz sandstones.³ In contrast, the $\delta^{18}\text{O}$ value for feldspar lies within the range that is typical for unaltered igneous rocks (6.3–8.3‰).²¹ The difference in $\delta^{18}\text{O}$ values between quartz and K-feldspar within trinitite is ~2‰, which suggests fractionation occurred at relatively high temperatures (comparable to an igneous system)⁵ assuming equilibrium conditions. The higher $\delta^{18}\text{O}$ values for “feldspar + clay” trinitite glass may be attributed to the presence of precursor minerals within the desert sand that are typically characterized by “heavy” oxygen isotope values due to their formation at low temperature, such as calcite, gypsum, and clay mineral phases.²²

Trinitite’s chemical composition is highly heterogeneous and is dependent on the relative abundance of the constituent minerals present within the precursor desert sand.¹³ While quartz and feldspar were not completely melted during the nuclear explosion, it also occurs as a type of glass melt along with the feldspathic + clay glass (Figure 2).⁷ On the basis of the major elements contained within the constituent minerals (e.g., quartz, calcite, gypsum, feldspar) along with trace minerals (e.g., ilmenite, amphibole, zircon, monazite, apatite) within the desert sand, trends or correlations in bivariate elemental plots can be interpreted to represent possible mixing relationships between these minerals. For example, both sodium and iron

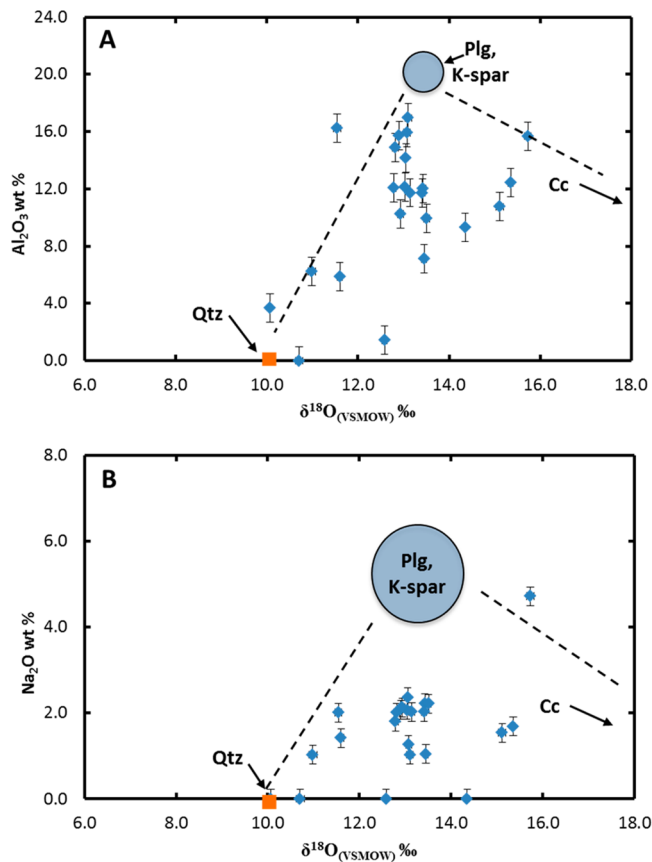


Figure 7. Al₂O₃ (A) and Na₂O (B) weight percent vs δ¹⁸O (in ‰, VSMOW) values of trinitite grains. Compositional fields for quartz (Qtz), feldspar (Plg, K-spar) melt, and calcite (Cc) are shown. Error bars are 1σ.

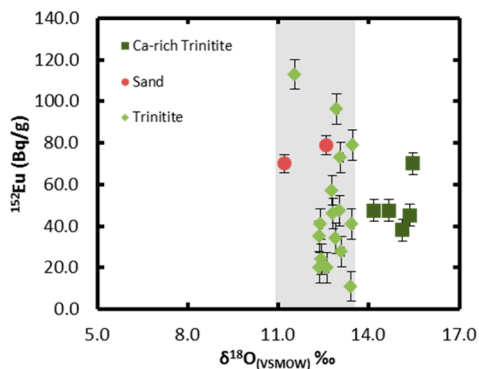


Figure 8. Plot of ¹⁵²Eu (units are Bq/g normalized to time of detonation) vs δ¹⁸O (in ‰, VSMOW) values of trinitite grains. "Ca-rich" trinitite samples contain >8 wt % CaO.

contents are positively correlated with aluminum abundances (Figure 4A,B) and may be attributed to the presence of varying proportions of amphibole. However, the presence of Fe-rich trinitite melt glass that is devoid of Na indicates the presence of an additional Fe-rich component that may be of anthropogenic origin (Figure 4C), such as the steel from the blast tower. A detailed SEM-EDS investigation of the melted surface of trinitite revealed the presence of micrometer-sized (10–100 μm) Fe-Ti inclusions, which have been interpreted to derive from the blast tower¹¹ and is consistent with previous investigations of trinitite.^{8,14}

The compositional heterogeneity of the various melt glasses within trinitite can be further evaluated by comparing the major element compositions with their corresponding oxygen isotope values. Figures 6 and 7 clearly show that the differences in the δ¹⁸O values for the various trinitite glasses can be correlated with their chemical compositions. Figure 6B illustrates that SiO₂ contents are inversely correlated with oxygen isotope values, whereas the latter are in general positively correlated with CaO wt % abundances (Figure 6A). The latter correlation may be in large part attributed to the input of calcite, which is present in the original sand, and this interpretation is corroborated by the high δ¹⁸O value reported for the loosely bound calcite component (Figure 6A; Table 1). Moreover, the variation in δ¹⁸O values for trinitite can be explained by the mixing of quartz, plagioclase (and K-feldspar), and calcite (Figures 6 and 7). Overall, it is clear that the trends observed between the abundances of major elements and stable oxygen isotope values (Figures 6 and 7) are dependent on the presence of quartz, feldspar, carbonate, and clay components within the trinitite melt glass.

The radioactive isotope ¹⁵²Eu, which is a neutron activation product from ¹⁵¹Eu present within the precursor arkosic sand at the Trinity site, is detectable in almost all samples of trinitite (from Bellucci et al.).¹⁶ In turn, the ¹⁵²Eu activity has been used to determine the spatial context of the trinitite samples relative to GZ¹⁶ which is a method adopted from previous investigations of trinitite (e.g., Parekh et al.; Belloni et al.).^{10,12} Figure 8 shows that there is a lack of correlation between the bulk rock activities of ¹⁵²Eu and corresponding oxygen values for the trinitite samples investigated here. However, all the trinitite melt glass samples and loose, unmelted sand components obtained from the underside of samples plot within a more restricted range of δ¹⁸O values (between 11 and 13.5‰; Figure 8), despite having relatively large differences in calculated ¹⁵²Eu values (10–115 Bq/g, normalized to time of detonation). This result suggests that the nuclear explosion did not significantly alter the inherent oxygen isotopes of the samples. As discussed above and demonstrated in Figures 6 and 7, the stable oxygen isotope results are clearly a function of the major chemical element of the samples, which can be related to the presence of constituent and trace minerals present within the arkosic sand at the Trinity site.

CONCLUSIONS

The major element compositions and stable oxygen isotope values reported here for various melt glass types within samples of trinitite are significantly correlated. This strongly suggests that the stable oxygen isotope values for trinitite melt glass are mainly dependent on the minerals present within the arkosic sand at the Trinity test site, and these were not significantly altered by the nuclear explosion. Stable isotope data for both "quartz" melt glass and intact K-feldspars are characterized by the lightest values. The higher δ¹⁸O values recorded for the remaining samples of trinitite melt glass may be attributed to the addition of minerals present in trace amounts, such as calcite, and clay group minerals.

ASSOCIATED CONTENT

S Supporting Information

Additional information as noted in text. This material is available free of charge via the Internet at <http://pubs.acs.org/>.

AUTHOR INFORMATION

Corresponding Author

*E-mail: ekoeman@nd.edu. Phone: 574-631-5380.

Author Contributions

The manuscript was written through contributions of all authors. All authors have given approval to the final version of the manuscript.

Notes

The authors declare no competing financial interest.

ACKNOWLEDGMENTS

We are extremely appreciative of the assistance, guidance, and expertise provided by Professor Zack Sharp (University of New Mexico) during his time spent at the University of Notre Dame installing the silicate extraction line and setting up the laser fluorination method employed here. The authors thank undergraduate students Timothy Hainley, Madeline Smierciak, Nolan Welsh, and Trinity Greenlawn high school student Courtney Morin with assistance in laser fluorination sample analysis. Technical assistance from Dennis Birdsell, Jon Loftus, and Suzyanne Guzicki (CEST) and Ginger Sigmon (EFRC) is gratefully acknowledged. This work is funded by DOE/NNSA Grant PDP11-40/DE-NA0001112.

REFERENCES

- (1) Sharp, Z. D. *Geochem. Cosmochim. Acta* **1990**, *54*, 1353–1357.
- (2) Silverman, S. R. *Geochem. Cosmochim. Acta* **1951**, *2*, 26–42.
- (3) Sharp, Z. *Principles of Stable Isotope Geochemistry*, first ed.; Pearson/Prentice Hall: Upper Saddle River, NJ, 2007.
- (4) Bottinga, Y.; Javoy, M. *Earth Planet. Sci. Lett.* **1973**, *20*, 250–265.
- (5) Clayton, R. N. In *Advances in Physical Geochemistry*; Newton, R. C., Navrotsky, A., Wood, B. J., Eds.; Springer-Verlag: Berlin, 1981; p 85–109.
- (6) Zheng, Y.-F. *Geochem. Cosmochim. Acta* **1991**, *57*, 1079–1091.
- (7) Ross, C. S. *Am. Mineral.* **1948**, *33*, 360–362.
- (8) Eby, N.; Hermes, R.; Charnley, N.; Smoliga, J. A. *Geol. Today* **2010**, *26* (5), 180–185.
- (9) Wallace, C.; Bellucci, J. J.; Simonetti, A.; Hainley, T.; Koeman, C.; Burns, P. C. *J. Radioanal. Nucl. Chem.* **2013**, *298*, 993–1003.
- (10) Belloni, F.; Himbert, J.; Marzocchi, O.; Romanello, V. *J. Environ. Radioact.* **2011**, *102*, 852–862.
- (11) Bellucci, J. J.; Simonetti, A. *J. Radioanal. Nucl. Chem.* **2012**, *293*, 313–319.
- (12) Parekh, P.; Semkow, T.; Torres, M.; Haines, D.; Cooper, J.; Rosenberg, P.; Kitto, M. *J. Environ. Radioact.* **2006**, *85*, 103–120.
- (13) Bellucci, J. J.; Simonetti, A.; Koeman, E. C.; Wallace, C.; Burns, P. C. *Chem. Geol.*, in press.
- (14) Fahey, A. J.; Zeissler, C. J.; Newbury, D. E.; Davis, J.; Lindstrom, R. M. *Proc. Natl. Acad. Sci. U. S. A.* **2010**, *107*, 20207–20212.
- (15) Wahl, A. C. *At. Data Nucl. Data Tables* **1988**, *39* (1), 1–156.
- (16) Bellucci, J. J.; Wallace, C.; Koeman, E. C.; Simonetti, A.; Burns, P. C.; Kieser, J.; Port, E.; Walczak, T. *J. Radioanal. Nucl. Chem.* **2013**, *295* (3), 2049–2057.
- (17) Hoefs, J. *Stable Isotope Geochemistry*, fourth ed.; Springer-Verlag: Heidelberg, 1997.
- (18) Jourdan, A. L.; Vennemann, T. W.; Mullis, J.; Ramseyer, K. *Mineral. Mag.* **2009**, *73*, 615–632.
- (19) Eiler, J.; Stolper, E. M.; McCanta, M. C. *J. Petrol.* **2011**, *52* (7&8), 1393–1413.
- (20) Paul, D.; Skrzypek, G.; Fórízs, I. *Rapid Commun. Mass Spectrom.* **2007**, *21*, 3006–3014.
- (21) Taylor, H. P., Jr. *Contrib. Mineral. Petrol.* **1968**, *19*, 1–71.
- (22) Savin, S. M.; Epstein, S. *Geochem. Cosmochim. Acta* **1970**, *34*, 35–42.
- (23) Eiler, J.; Stolper, E. M.; McCanta, M. C. *J. Petrol.* **2011**, *52* (7&8), 1393–1413.